Nanostructured Organic Semiconductors *via* Directed Supramolecular Assembly

Benjamin J. Rancatore,[†,‡,§,¶] Clayton E. Mauldin,[†,¶] Shih-Huang Tung,[‡] Cheng Wang,[⊥] Alexander Hexemer,[⊥] Joseph Strzalka,[∥] Jean M. J. Fréchet,[†,§,*] and Ting Xu[†,‡,§,*]

[†]College of Chemistry, and [‡]Department of Materials Science and Engineering, University of California, Berkeley, California 94720-1460, [§]Material Sciences Division, and [⊥]Advanced Light Source, Lawrence Berkeley National Laboratory, Berkeley, California 94720, and [∥]X-Ray Science Division, Argonne National Laboratory, Argonne, Illinois 60439. [¶]These authors contributed equally to this work.

ABSTRACT Organic small molecule semiconductors have many advantages over their polymer analogues. However, to fabricate organic semiconductor-based devices using solution processing, it is requisite to eliminate dewetting to ensure film uniformity and desirable to assemble nanoscopic features with tailored macroscopic alignment without compromising their electronic properties. To this end, we present a modular supramolecular approach. A quaterthiophene organic semiconductor is attached to the side chains of poly(4-vinylpyridine) *via* noncovalent hydrogen bonds to form supramolecular assemblies that act as p-type semiconductors in field-effect transistors. In thin films, the quaterthiophenes can be readily assembled into microdomains, tens of nanometers in size, oriented normal to the surface. The supramolecules exhibited the same field-effect mobilities as that of the quaterthiophene alone (10^{-4} $cm^2/(V \cdot s)$). Since the organic semiconductors can be readily substituted, this modular supramolecular approach is a viable method for the fabrication of functional, nanostructured organic semiconductor films using solution processing.

KEYWORDS: organic semiconductor · supramolecular assembly · thin film · charge mobility

Small molecule organic semiconductors have many advantages over their polymer analogues, including their high purity and well-defined electronic properties.[1−4] They provide unique opportunities to fabricate low-cost, high-performance organoelectronic devices such as organic photovoltaics (OPVs) or organic light-emitting diodes (OLEDs).[1,5−8] However, it remains a challenge to solution process them into uniform films, due to dewetting and their strong tendency to crystallize.[2,9] In blends of electron donors and acceptors, one major hurdle is to assemble each type of the functional small molecules into nanoscopic grains, tens of nanometers in size so as to increase donor/acceptor interfaces.[10−12] To effectively transport charges to the electrodes, these nanoscopic grains need to be macroscopically oriented normal to the surface, and the orientation and molecular packing of the organic semiconductors within each grain need to be tailored.[10]

Various approaches have been explored to overcome these barriers. Conjugated polymers are amenable to solution processing and are used extensively,[12−15] though they typically exhibit mobilities lower than their small molecule counterparts.[16] To date, solution-processable OPVs with power conversion efficiencies of ~5−6% were achieved by kinetically trapping the spinodal decomposition of the active layer, that is, a blend of conjugated polymer and organic semiconductor.[17−19] The main remaining concern is to obtain ideal morphologies for OPVs with nanoscopic features with sizes comparable to typical exciton diffusion lengths that are vertically aligned to allow charges to reach electrodes.[18] Block copolymers (BCPs) microphase separate and form well-defined arrays of microdomains, tens of nanometers in size. In thin films, BCP microdomains can be oriented normal to the surface by applying an external surface, electric or solvent field.[20−22] However, such fine morphological control cannot be achieved with conjugated BCPs due to their poor solubility, low chain mobility, and high tendency to aggregate.[23−28] Electronic properties can also be built-in through the covalent attachment of conjugated molecules to the side chains of BCP blocks.[23,29] However, the generality is limited because the synthesis of such BCPs is challenging, as monomers containing conjugated molecules have limited solubility. The covalently linked side groups may also reduce the mobility of the polymer chain and restrain the molecular packing of the attached conjugated molecules required for high charge mobility.

BCP-based supramolecules can be constructed by attaching small molecules to

*Address correspondence to tingxu@berkeley.edu, frechet@berkeley.edu.

Received for review March 13, 2010 and accepted April 05, 2010.

Published online April 19, 2010. 10.1021/nn100521f

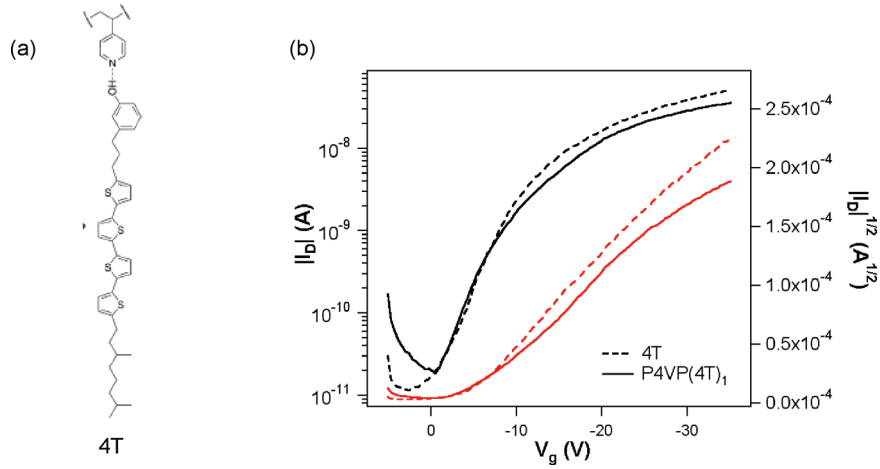

Figure 1. (a) Chemical structure of phenol−pyridine hydrogen bond between 4T and the 4-vinylpyridine unit of a P4VP polymer. (b) Plot of $|I_D|$ for a thermally annealed 4T (dashed line) device with $W = 400$ μm and $L = 10$ μm and a solvent-annealed P4VP(4T)$_1$ device with $W = 400$ μm and $L = 20$ μm. The charge mobilities for both devices were calculated to be 10^{-4} cm^2/(V · s), and on/off ratio of the devices were 10^3.

pendant functionalities of a polymer chain *via* hydrogen bonding, electrostatic interactions, or metal ligation.[30−38] The coil-comb supramolecules phase separate into arrays of well-defined microdomains similar to those seen in BCP alone, and small molecules order within BCP microdomains. In thin films of BCP-based supramolecules, the macroscopic orientation of supramolecular assemblies can be tailored.[39−43] Experimentally, by adjusting the loading of the small molecules, the BCP microdomains can be aligned perpendicular to the surface.[41,43] Within BCP microdomains, lamellar assemblies from the comb block, several nanometers in size, are oriented parallel to the surface and small molecules are aligned perpendicular to the surface.[41,43] Blending organic semiconductors with inert polymers was shown to be effective for improving the solution processability of the semiconductor.[44] The supramolecular approach provides a new avenue to solution process organic semiconductors as well as to assemble them into nanoscopic structures in thin films. It circumvents some of the synthetic challenges inherent to the preparation of conjugated BCPs and enables the tailoring of electronic properties without the need to synthesize new polymers.[34] Kinetically, the noncovalent linking of an organic semiconductor to a BCP block preserves the chain mobility of the polymer necessary for ordered self-assembly during annealing, while constraining crystallization of the small molecule to within the microdomains. Indeed, nanostructured thin films were recently obtained in blends of regioregular poly(3-hexylthiophene)-*block*-poly(4-vinylpyridine) rod−coil block copolymers with [6,6]-phenyl-C61-butyric acid methyl ester (PCBM).[45] Favorable interactions between PCBM and P4VP sequestered PCBM within BCP microdomains and led to bicontinuous electron donor/electron acceptor networks with high thermal stability.

RESULTS AND DISCUSSION

We construct supramolecules by attaching oligothiophene organic semiconductors to the polymer side chains *via* hydrogen bonding and investigate critical parameters governing their assembly and electronic properties.[30,33,46] 5′′′-(3,7-Dimethyloctyl)-5-(3-(3-hydroxyphenyl)propyl)-[2,2′;5′,2′′;5′′,2′′′] quaterthiophene, a semiconductor with a pendant phenol moiety identified as **4T**, was designed to hydrogen bond to the 4-vinylpyridine units of a poly(4-vinylpyridine) (46.7 kDa), as shown in Figure 1a.[33] The resultant supramolecules are identified as P4VP(**4T**)$_r$ (in which r denotes the ratio of **4T** to the 4VP unit). As mentioned, the end group of **4T** is a phenolic moiety that hydrogen bonds to the pyridyl side chains of the polymer; this is attached through a short spacer to the semiconducting quaterthiophene with a terminal alkyl group.

Differential scanning calorimetry (DSC) reveals a pair of endotherms at 126 and 138 °C upon heating and exotherms at 142 and 106 °C upon cooling (see Supporting Information Figure S1). The H-bond between the phenol group and the 4VP becomes unstable at temperatures above 110 °C and remains present even up to 190 °C.[47] The melting temperature of **4T** is, therefore, within the temperature range necessary to access **4T**'s amorphous state without completely breaking its noncovalent link to the BCP side groups. This provides mobility to the P4VP(**4T**)$_r$ block while preserving the integrity of the hierarchical assemblies.

The **4T** molecule is highly soluble in numerous organic solvents, but uniform films cannot be formed by spin-coating. In addition, **4T** dewets the Si substrate upon thermal annealing. For a small fraction of functional organic field-effect transistor (OFET) devices, thermal annealing of the **4T** films at 135 °C for 10 min produced a linear plot of $|I_D|^{1/2}$ in transfer $I-V$ curves where

I_D is the current measured at the drain electrode, shown in Figure 1b, and charge mobilities of 10^{-4} $cm^2/(V \cdot s)$. The charge mobilities of **4T** are much lower than that of semiconducting liquid-crystalline thieno[3,2-*b*]thiophene polymers that form large crystalline domains and have shown charge-carrier mobilities as high as 1 $cm^2/(V \cdot s)$.[13,48] Yet, they are comparable to or higher than many conjugated polymers that have been used in OLEDs and OPVs.[25,49−51] Low off-currents, the minimum I_D measured in the devices, suggest a low level of doping in the pristine small molecule films.[2] Furthermore, devices exhibited a low turn-on voltage, which suggests a low barrier to mobile charge injection.

Having validated **4T** as an organic semiconductor in p-channel OFETs, we studied the charge transporting capabilities of the P4VP(**4T**)$_1$ supramolecule. Analysis of OFET data enables the calculation of charge mobility for the organic semiconductor and also provides for a qualitative evaluation of the level of dopants and charge traps introduced into the films during the process of supramolecule formation. Top-contact and bottom-gate devices were prepared to ensure that the P4VP(**4T**)$_1$ could provide conductive pathways in OFET channels, which is important for fabricating OPV devices. While the **4T** films were observed to dewet the device substrates, decreasing the OFET device yield, uniform films of controlled thicknesses were readily cast from the P4VP(**4T**)$_1$. High-quality thin films can also be processed for $r > 1$. Thin films of P4VP(**4T**)$_1$, ~60 nm in thickness, were solvent-annealed under chloroform vapor for 24 h to improve the ordering of P4VP(**4T**)$_1$. As shown in a representative transfer $I-V$ plot in Figure 1b, the solvent-annealed P4VP(**4T**)$_1$ films functioned as the active layer in OFETs with charge mobilities of 10^{-4} $cm^2/(V \cdot s)$. The saturation current levels were similar to those obtained in annealed pristine **4T** OFETs, and off-currents remained low. Since P4VP preferentially interacts with silicon oxide and the **4T** molecule dewets the silicon substrate, the higher affinity of P4VP to silicon oxide layer precludes the **4T** enrichment at the P4VP(**4T**)$_1$/SiO_2 interface.[39] Thus, the OFETs measure the mobility of charge in a thin layer (~5−10 nm) of the P4VP(**4T**)$_1$ next to the SiO_2 dielectric, not phase-separated **4T**.[52,53]

The ordering and spatial arrangements of P4VP(**4T**)$_1$ in thin films were characterized by the grazing incidence small-angle X-ray scattering (GISAXS) to correlate the structure−function relationship. The incidence angles (α_{in}) are in the range of 0.15−0.20°, and the incident X-rays penetrate the whole film and probe structural information throughout the film. Figure 2a shows the GISAXS pattern of a similar solvent-annealed P4VP(**4T**)$_1$ film, and the q_z scan is shown in Figure 2b. Diffraction spots, instead of diffraction rings, are seen in the q_z direction, indicating that the P4VP(**4T**)$_1$ forms lamellar domains, ~6.3 nm in periodicity, and are mainly oriented parallel to the substrate. Thermal annealing at 110 °C for 1 h enhances the P4VP(**4T**)$_1$ ordering and sharpened the diffraction peaks, as seen in the q_z scan also shown in Figure 2b. This macroscopic alignment of **4T** as schematically shown in the inset of Figure 2b is similar to that seen in thin films of oligothiophenes alone.[54]

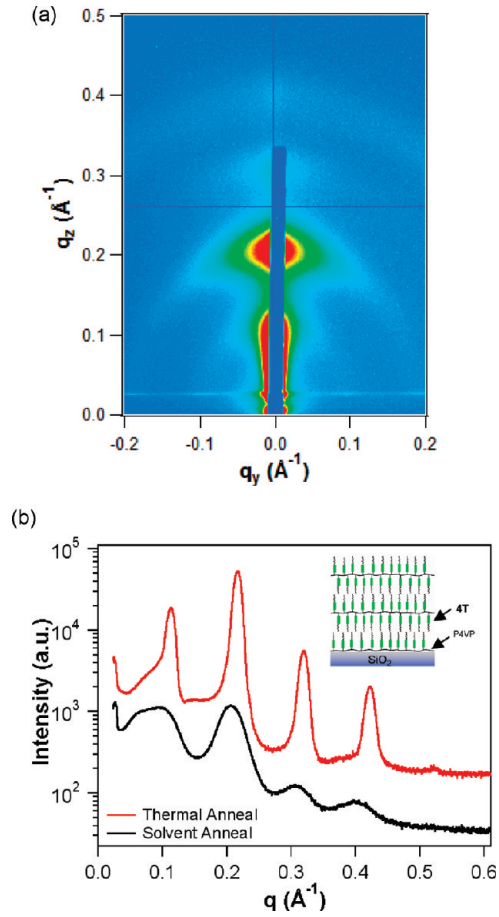

Figure 2. (a) GISAXS pattern at an incident angle of ~0.15° and (b) the q_z scan (black) at $q_y = 0.017$ Å^{-1} of a ~60 nm P4VP(4T)$_1$ thin film after solvent annealing for 36 h, showing the P4VP(4T)$_1$ lamellae, ~6.3 nm in periodicity, are oriented parallel to the surface as schematically shown in the inset of (b). Thermal annealing at 110 °C for 1 h enhanced the P4VP(4T)$_1$ ordering and sharpened the diffraction peaks as seen in the q_z scan (red) shown in (b).

A bottom-gate and top-contact test structure requires a film with semiconducting properties through its entire thickness for measurement of gate-modulated current.[44] Thus, the OFET and GISAXS results clearly demonstrated that, by hydrogen bonding **4T** to P4VP, P4VP(**4T**)$_1$ thin films transport charges in both the lateral and vertical directions. Constructing the P4VP(**4T**)$_1$ supramolecule does not sacrifice charge mobility of **4T**, yet enables solution processing of oligothiophenes into uniform films with control over the spatial arrangements of **4T**.

Hydrogen bonding **4T** to a BCP, poly(styrene)(40K)-*block*-poly(4-vinylpyridine)(5.6K) (PS-*b*-P4VP) results in a BCP-based supramolecule, PS-*b*-P4VP(**4T**)$_r$. The synergistic co-assembly of BCP and **4T** may lead to

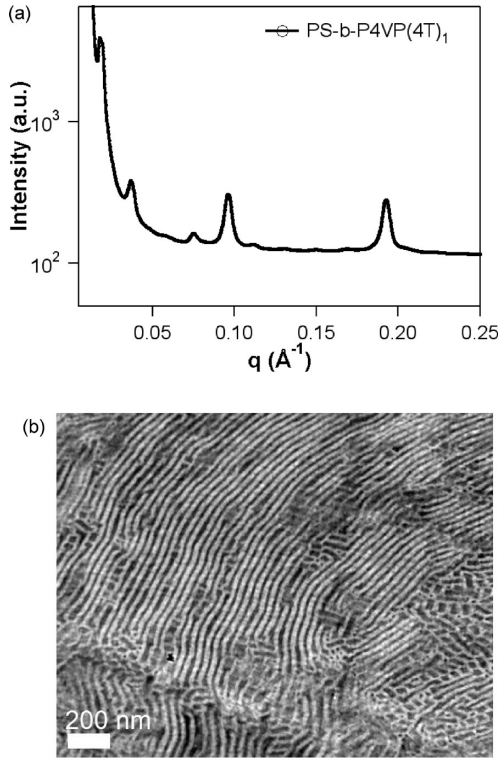

Figure 3. (a) SAXS profile and (b) TEM image of PS-*b*-P4VP(4T)$_1$ annealed at 110 °C, showing a lamellae-within-lamellae morphology.

hierarchical assemblies that may satisfy many morphological requirements for high-efficiency OPVs and OLEDs.[10−12] However, most of previous studies on BCP-based supramolecules focused on small molecules which have a much weaker tendency to aggregate in comparison to **4T**.[44] For highly crystalline organic semiconductors, such as **4T**, the crystallization may induce phase separation. A delicate balance between BCP self-assembly and crystallization of the semiconductor is required to obtain the desired hierarchical assemblies. Thus, we first investigated the assembly of PS-*b*-P4VP(**4T**)$_r$ in bulk, which provided guidance to manipulate **4T** assemblies in thin films.

Figure 3a,b shows the small-angle X-ray scattering (SAXS) profile and transmission electron microscopy (TEM) image of PS-*b*-P4VP(**4T**)$_1$ annealed at 110 °C. The annealing temperature is selected because the hydrogen bonding between **4T** and 4VP becomes unstable at temperatures above 110 °C.[47] The SAXS profile confirmed a lamellae-within-lamellae hierarchical assembly where the BCP forms a lamellar morphology with a periodicity of ~33.7 nm and the P4VP(**4T**)$_1$ comb block forms lamellae with a periodicity of ~6.3 nm. The TEM image shows that **4T**s were completely incorporated within the BCP lamellae. The weight percentage of **4T** in PS-*b*-P4VP(**4T**)$_1$ is only 42%. The **4T** fraction needs to be increased to ensure charge injection and transport.

As r increases to 1.5, after annealing at 110 °C, the SAXS profile (Figure 4a) indicated the presence of nanostructures resulting from BCP microphase separation. Figure 4b shows a representative TEM image, and no large grains of **4T** phase-separated from BCP were observed. However, a mixture of two morphologies was observed, indicating non-uniform distribution of **4T**. On the right side, P4VP(**4T**)$_{1.5}$ microdomains appear to pack into hexagonal arrays embedded in the PS matrix. In the lamellar morphology region on the left-hand side of the image, many defects are seen and the ordering is poor. Interestingly, in many regions, as indicated by the circle in the inset, two BCP microdomains are connected with lamellae with much smaller periodicity of ~6 nm. It is highly likely that these lamellae are assemblies of **4T** alone and correspond to the diffraction peak at $q = \sim 0.011$ Å^{-1}. At $r > 1$, the excess amount of **4T** crystallizes during the drying process, leading to inhomogeneous distribution of **4T**. At 110 °C, below the melting temperature of **4T**, the mobility of PS-*b*-P4VP(**4T**)$_r$ is significantly reduced to achieve uniform supramolecular assemblies. Mixed morphologies were not observed previously in BCP-based supramolecules and can be attributed to **4T**'s strong tendency to crystallize.

Further increasing the thermal annealing temperature to 155 °C, above the melting temperature of **4T**, uniform lamellae-within-lamellae morphology was observed for PS-*b*-P4VP(**4T**)$_{1.5}$, as shown in Figure 4c. The SAXS profile in Figure 4a shows that the complete incorporation of **4T** into BCP lamellae increases the BCP periodicity to ~52 nm. Within BCP lamellar microdomains, the P4VP(**4T**)$_{1.5}$ comb blocks assemble into lamellae, ~6.4 nm in periodicity, and can be clearly seen. Although a fraction of hydrogen bonds were broken at 155 °C and $r > 1$, the favorable interaction between the phenolic end group of the semiconductor and the pyridyl side group of the BCP and strong $\pi-\pi$ interactions between the oligothiophenes provide sufficient driving force to sequester the oligothiophenes into BCP microdomains and prevent macrophase separation. For P4VP(**4T**)$_r$ thin films, grazing incidence X-ray scattering shows macrophase separation between **4T** and P4VP(**4T**)$_r$ upon increasing the **4T** to 4VP stoichiometry to $r = 1.5$. However, for PS-*b*-P4VP(**4T**)$_r$, similar morphologies were observed for $r = 2$ and $r = 1.5$ in bulk; that is, mixed morphologies were seen for supramolecules annealed at 110 °C, and lamellae-within-lamellae morphology was observed after thermal annealing at 155 °C. In thin films, similar GISAXS patterns were observed for PS-*b*-P4VP(**4T**)$_r$ at $r = 1.5$ and $r = 2$ after solvent annealing and thermal treatment, respectively.

The ideal morphology for OPV and OLED requires an alignment of BCP microdomains in thin films normal to the film surface. Upon attaching **4T** to the P4VP side chain, the BCP microdomain orientation depends on the interactions between each component with the underlying substrate. As shown in Figure 2b, favorable interactions between P4VP

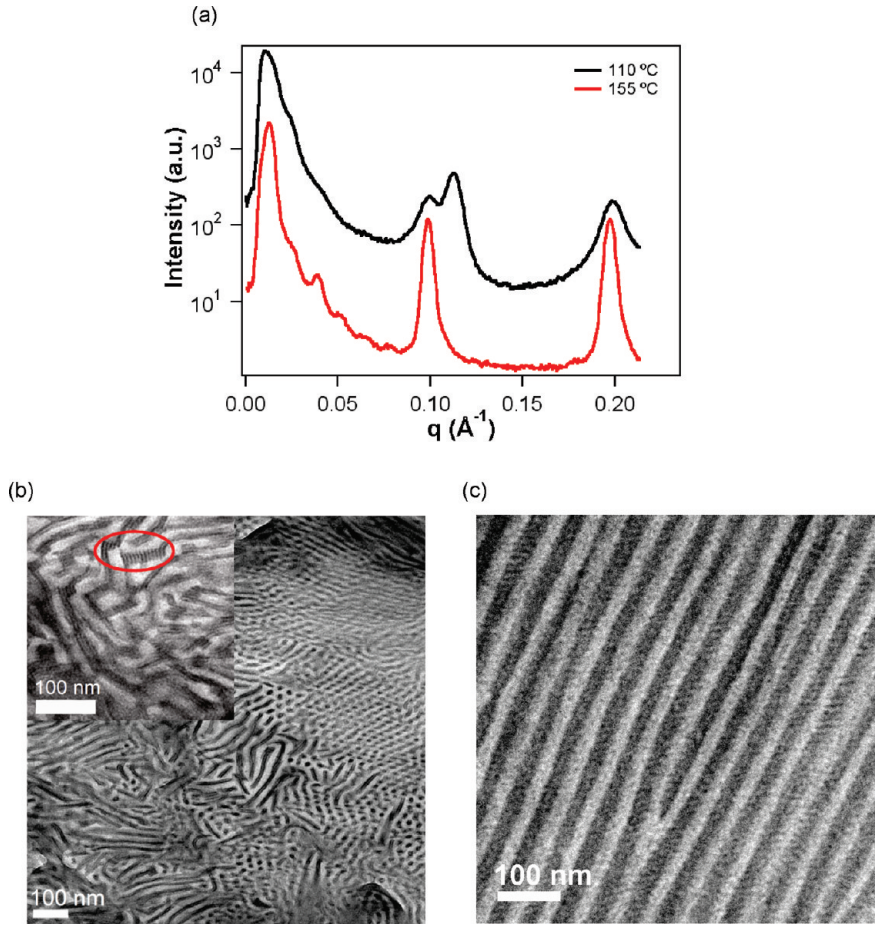

Figure 4. (a) SAXS profiles of PS-*b*-P4VP(4T)$_{1.5}$ annealed at 110 and 155 °C. The TEM images are shown in (b) and (c), respectively. For PS-*b*-P4VP(4T)$_{1.5}$ annealed at 110 °C, mixed morphologies were seen and 4T organizes into lamellae, ~6 nm in periodicity, and bridging BCP lamellae can be seen in the zoom-in TEM image in the inset of (b). After annealing at 155 °C, the P4VP(4T)$_{1.5}$ comb blocks assemble into lamellae, ~6 nm in periodicity, within BCP lamellar microdomains.

with the Si substrate orient the P4VP(**4T**)$_1$ lamellae parallel to the surface. For PS-*b*-P4VP(**4T**)$_1$ supramolecules, the parallel orientation of P4VP(**4T**)$_1$ lamellae may overcome the nonfavorable interactions between the PS block with the underlying substrate and induce the BCP microdomains to orient normal to the surface, as shown in Figure 5a.

Thin films of PS-*b*-P4VP(**4T**)$_r$, ~50 nm in thickness, were spin-coated onto silicon wafers with ~1000 Å thermally grown oxide layers and solvent-annealed in chloroform vapors. A comparative plot of saturation currents in solvent-annealed PS-*b*-P4VP(**4T**)$_{1.5}$ OFETs is shown in Figure 5b. The charge mobility of PS-*b*-P4VP(**4T**)$_{1.5}$ was calculated to be 10^{-4} cm^2/(V · s), which is comparable to **4T** and P4VP(**4T**)$_1$. The OFET results suggested that the P4VP(**4T**)$_r$ microdomains are oriented normal to the surface as further confirmed by GISAXS studies. Figure 5c shows the GISAXS pattern of a ~60 nm PS-*b*-P4VP(**4T**)$_{1.5}$ thin film after solvent annealing. At $\alpha_{in} = 0.20°$, features in both q_z and q_y directions are seen. The q_y scan only shows a broad diffraction peak at $q_y = \sim 0.017$ Å^{-1}, corresponding to the lateral microphase separation of PS-*b*-P4VP(**4T**)$_{1.5}$ with a periodicity of ~37 nm. The solvent-annealed PS-*b*-P4VP(**4T**)$_{1.5}$ film is microphase-separated with fairly poor lateral order. However, only diffraction spots, instead of rings, were seen in the GISAXS pattern, indicating that the BCP microdomains are mainly oriented normal to the substrate. Grazing incidence wide-angle X-ray scattering (GIWAXS) was used to investigate the ordering of PS-*b*-P4VP(**4T**)$_{1.5}$ at much smaller length scales, as seen in Figure 5d. At higher q_y direction, diffuse scattering originating from the molecular packing of **4T** can also be seen around q_y of 1.2−1.4 Å^{-1}.[54] As seen, the crystallinity of **4T** in thin films of PS-*b*-P4VP(**4T**)$_{1.5}$ is rather low. However, there are a series of diffraction peaks along the q_z direction, originating from the P4VP(**4T**)$_r$ lamellae with a periodicity of ~6.3 nm oriented parallel to the surface similar to that shown in the inset of Figure 2b. Thermal annealing at 110 °C for 1 h improved the hierarchical ordering of PS-*b*-P4VP(**4T**)$_{1.5}$ significantly and resulted in a sharpening of peaks in the q_y and q_z directions as shown in Figure 5e. GIWAXS also showed that the diffraction peaks associated with assemblies of P4VP(**4T**)$_1$ and **4T** alone sharpened significantly. The q_y scan shows that thermally annealed PS-*b*-P4VP(**4T**)$_{1.5}$ thin films formed BCP lamellae oriented normal to the film surface with a periodicity

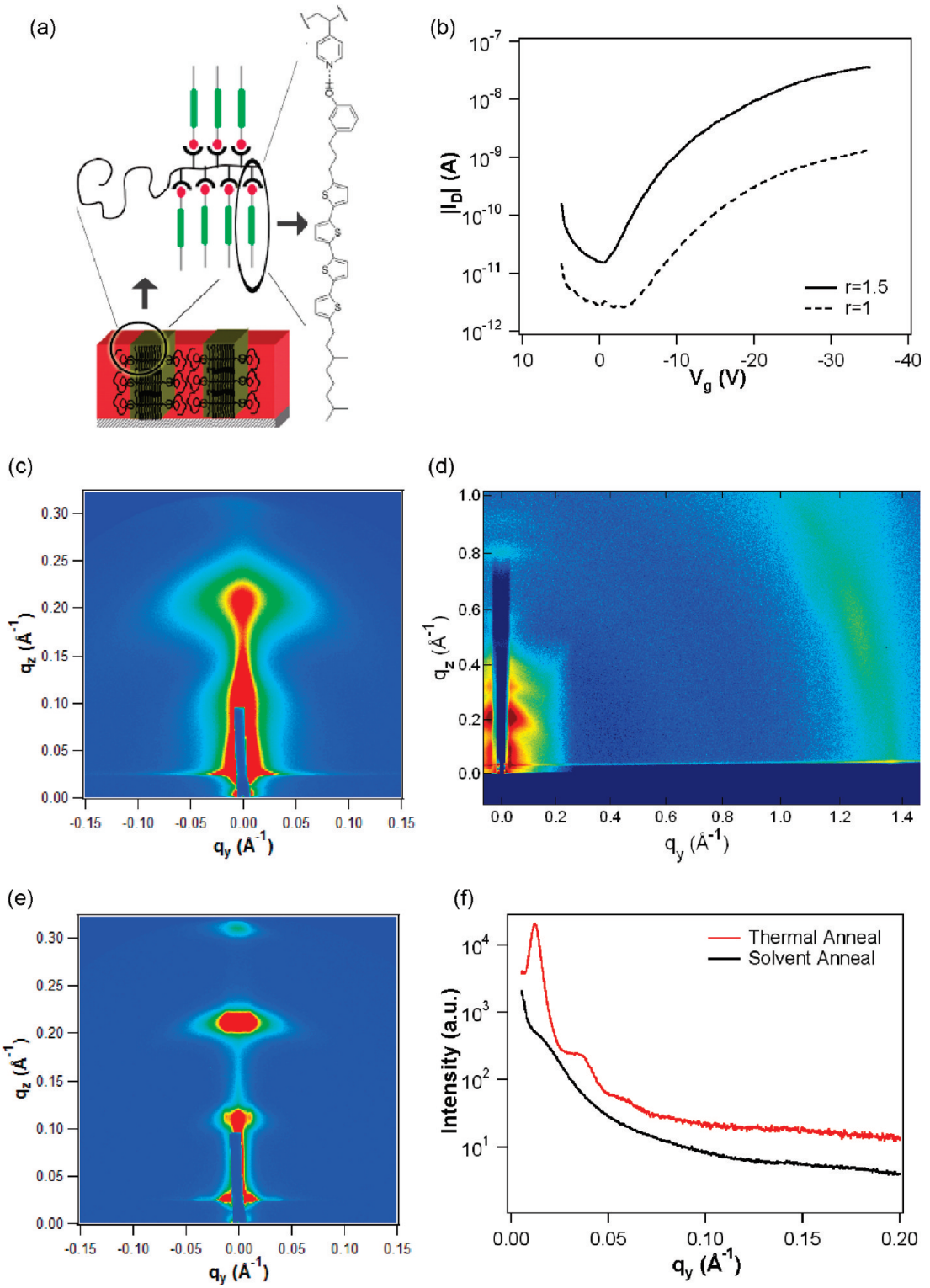

Figure 5. (a) Schematic drawing of ideal hierarchical assembly of PS-*b*-P4VP(4T), in thin films for OPV fabrication, where BCP microdomains are oriented normal to the surface. (b) Comparison of *I*−*V* plots for PS-*b*-P4VP(4T), OFETs, where $r = 1$ (dashed lines) and $r = 1.5$ (solid lines). The devices are the same geometry with $W = 200$ μm and $L = 10$ μm. The charge mobility was calculated to be 10^{-6} and 10^{-4} cm^2/(V · s) for $r = 1$ and 1.5, respectively. The on/off ratio for PS-*b*-P4VP(4T)$_{1.5}$ OFETs was 10^3. (c) GISAXS and (d) GIWAXS patterns of a ~50 nm PS-*b*-P4VP(4T)$_{1.5}$ thin film after solvent annealing for 24 h at incident angles of 0.19−0.2°. (e) GISAXS pattern of the same PS-*b*-P4VP(4T)$_{1.5}$ thin film after thermal annealing for 1 h at 100−110 °C under N_2. The q_y scan at an incident angle of 0.19° is shown in (f). With thermal annealing, the thin film of PS-*b*-P4VP(4T)$_{1.5}$ forms a hierarchical structure similar to that shown in (a), where BCP lamellae, ~52 nm in periodicity, are oriented perpendicular to the surface and P4VP(4T)$_{1.5}$ lamellae, ~6.3 nm in periodicity, are oriented parallel to the surface.

of ~52 nm and suggests a complete incorporation of **4T** into BCP lamellae. Thus, thermal-annealed thin films of PS-*b*-P4VP(**4T**)$_{1.5}$ form hierarchical structures similar to that schematically shown in Figure 5a. However,

OFET studies showed that the thermal treatment reduced the charge mobility of the PS-*b*-P4VP(**4T**)$_{1.5}$ thin films.

Thus, solvent-annealed PS-*b*-P4VP(**4T**)$_{1.5}$ does not form a well-ordered lamellae-within-lamellae morphology in thin films as previously found with other BCP-based supramolecules.[41,43] We speculate that, after solvent annealing, PS-*b*-P4VP(**4T**)$_{1.5}$ may form morphologies similar to that shown in Figure 4b, where a significant fraction of **4T**s organize into lamellae bridging the BCP lamellae in different grains to provide a pathway to transport charges between P4VP(**4T**)$_r$ lamellae. Upon thermal annealing, **4T**s are incorporated within P4VP(**4T**)$_r$ microdomains, which resulted in an increase in BCP periodicity. This improves macroscopic alignment of BCP lamellae normal to the surface, however, very likely removes the electronic pathway and reduces charge mobility.[55]

CONCLUSIONS

We have shown that a molecular design strategy involving the noncovalent linking of organic semiconductors to a polymer chain successfully allows solution processing and ordering of semiconductor molecules into hierarchical assemblies with macroscopic alignment of the organic semiconductor in thin films. The supramolecular comb block, P4VP(**4T**)$_r$, transports charge in OFET channels, making these films act as nanostructured semiconductor composites. Although effectively measuring the mobility of charge in a thin layer (~5−10 nm) of the organic semiconductor next to the SiO_2 dielectric instead of the bulk property,[52,53] the top-contact, bottom-gated OFET experiments demonstrate the functionality of the supramolecular film assemblies. Additionally, the charge mobilities of **4T** and P4VP(**4T**)$_r$ measured in OFETs are comparable to organic semiconductors that have been use in OLEDs[56] and OPVs.[25,49] This mobility value is greater than that measured in some conjugated polymers, such as poly(*p*-phenylene vinylene), where nanoscopic assembly is challenging.[50,51] The presented supramolecular approach and design principle should be applicable to other organic semiconductors and thus provide a versatile method to access films with spatial and orientational control of the semiconductor, which is otherwise difficult. Furthermore, recent studies have shown that BCP-based supramolecules can effectively organize semiconductor nanoparticles into ordered arrays, which provides a viable and effective means to incorporate electron donor or acceptors as needed.[57] This, in conjunction with the use of other small molecules with improved electronic properties, may potentially lead to the fabrication of high-performance OPVs and OLEDs.

METHODS

Materials. P4VP(46 700 Da) (PDI = 1.14) and PS(40 000 Da)-*b*-P4VP(5600 Da) (PDI = 1.09) were purchased from Polymer Source, Inc. Chloroform was purchased from Fisher and filtered through basic alumina. All other chemicals were purchased from Aldrich and used as received. Synthetic procedure to prepare **4T** is described in detail in the Supporting Information.

Sample Preparation. The PS-*b*-P4VP or the P4VP was first dissolved in chloroform to form 1−2% (w/v) stock solutions. The desired amount of **4T** was dissolved in chloroform. The polymer solution was then added to the **4T** solution, followed by stirring overnight. Thin films were prepared by spin-coating the mixed solutions onto silicon wafers at spinning speeds between 1000 and 4000 rpm. **4T** is light and oxygen-sensitive, and so cautions were paid to avoid light exposure during the sample preparation process. Sample thicknesses were measured using a Filmetrics-sTM F20 interferometer. For solvent annealing, thin films were placed together with a beaker of 40 mL of chloroform at 22 °C inside an inverted dish (170 diameter × 90 height mm) on which a ~2 kg weight was loaded for 24−48 h. For thermal annealing, samples were wrapped in aluminum foil inside an inverted dish and placed in an oven under a nitrogen atmosphere at 100−110 °C for 1 h.

SAXS and GISAXS. Bulk samples were prepared by casting and drying the supramolecule solutions in a Teflon beaker, inside an inverted dish, and allowing the solvent to evaporate over 48 h. Samples were then thermally annealed at ~100−110 or 155 °C under vacuum overnight and then slowly cooled to room temperature. The SAXS data were collected on beamline 7.3.3 in the Advanced Light Source (ALS) at the Lawrence Berkeley National Laboratory. X-rays, with a wavelength of 1.240 Å (10 keV), were used, and the scattering spectra were collected on an ADSC Quantum 4u CCD detector with an active area of 188 mm × 188 mm (2304 × 2304 pixels) and a dynamic range of 16 bit. The scattering profiles, after a 20 s collection time, were obtained by integrating the 2-D scattering pattern. GISAXS measurements were made on beamline 7.3.3 in ALS and beamline 8-ID-E[58] in the Advanced Photon Source (APS) at the Argonne National Laboratory. X-ray wavelengths of 1.240 Å (ALS) and 1.687 Å (APS) were used. The scattering profiles were collected on a Mar 165 CCD at APS and an ADSC Quantum 4u CCD detector at ALS. GIWAXS measurements were made at beamline 8-ID-E of the APS using a Pilatus 100K pixel array detector approximately 270 mm from the sample and mounted on a linear stage that translated the detector horizontally transverse to the beam. The two-dimensional image is a composite of six exposures joined together so as to eliminate overlapping regions between the images. Line-averaged intensities are reported as *I versus q*, where $q = (4\pi/\lambda) \times \sin(\theta/2)$, λ is the wavelength of incident X-rays, and θ is the scattering angle.

Transmission Electron Microscopy (TEM). The same samples used for SAXS were embedded in resin and cured at 60 °C overnight before being microtomed for TEM imaging. The thin sections of PS(40 000)-*b*-P4VP(5600)(**4T**)$_1$ were exposed to iodine vapor for 10 min that selectively stains the P4VP(**4T**)$_r$ block to enhance the contrast. TEM images were collected on a FEI Tecnai 12 transmission electron microscope at an accelerating voltage of 120 kV.

OFET Fabrication. The devices were fabricated on low resistivity n-type silicon wafers, using 1000 Å of thermally grown SiO_2 as the dielectric, in top-contact geometry. Sample thin films were prepared as previously described. Gold contacts were patterned on top of the films, using various shadow masks, giving channel lengths from 5 to 40 μm and widths from 200 to 400 μm. All devices were tested as p-type OFETs in the accumulation regime, and saturation mobilities were calculated using the equation, $\mu = g_m^2/2I_DC_{ox}(W/L)$, where g_m = transconductance, I_D = current measured at the drain electrode, C_{ox} = capacitance of the insulator, W = width of the electrodes, and L = channel length. The electrical measurements were performed in a nitrogen atmosphere using an Agilent 4156C Precision semiconductor parameter analyzer.

Acknowledgment. This work was supported by the National Science Foundation through the Center of Integrated Nanomechanical Systems under Grant No. EEC-0832819 (B.J.R. and S.-H.T.) and under Grant No. NSF-DMR-0906638 (C.E.M. and J.M.J.F.). This work is also supported by the Director, Office of Science, Office of Basic Energy Sciences, Materials Sciences and Engineering Division, of the U.S. Department of Energy under Contract No. DE-AC02-05CH11231 (J.M.J.F. and T.X.). The Advanced Light Source is supported by the Director, Office of Science, Office of Basic Energy Sciences, of the U.S. Department of Energy under Contract No. DE-AC02-05CH11231 (C.W. and A.H.). Use of the Advanced Photon Source was supported by the U.S. Department of Energy, Office of Science, Office of Basic Energy Sciences, under Contract No. DE-AC02-06CH11357 (J.S.).

Supporting Information Available: Complete experimental procedures and characterization of **4T** and synthetic intermediates. DSC results for **4T**. This material is available free of charge *via* the Internet at http://pubs.acs.org.

REFERENCES AND NOTES

1. Peumans, P.; Yakimov, A.; Forrest, S. R. Small Molecular Weight Organic Thin-Film Photodetectors and Solar Cells. *J. Appl. Phys.* **2003**, *93*, 3693–3723.
2. Katz, H. E.; Bao, Z.; Gilat, S. L. Synthetic Chemistry for Ultrapure, Processable, and High-Mobility Organic Transistor Semiconductors. *Acc. Chem. Res.* **2001**, *34*, 359–369.
3. Rand, B. P.; Xue, J. G.; Yang, F.; Forrest, S. R. Organic Solar Cells with Sensitivity Extending into the Near Infrared. *Appl. Phys. Lett.* **2005**, *87*, 233508.
4. Peumans, P.; Uchida, S.; Forrest, S. R. Efficient Bulk Heterojunction Photovoltaic Cells Using Small-Molecular-Weight Organic Thin Films. *Nature* **2003**, *425*, 158–162.
5. Riede, M.; Mueller, T.; Tress, W.; Schueppel, R.; Leo, K. Small-Molecule Solar Cells—Status and Perspectives. *Nanotechnology* **2008**, *19*, 424001.
6. Matsuo, Y.; Sato, Y.; Niinomi, T.; Soga, I.; Tanaka, H.; Nakamura, E. Columnar Structure in Bulk Heterojunction in Solution-Processable Three-Layered P-I-N Organic Photovoltaic Devices Using Tetrabenzoporphyrin Precursor and Silylmethyl[60]Fullerene. *J. Am. Chem. Soc.* **2009**, *131*, 16048–16050.
7. Roncali, J. Molecular Bulk Heterojunctions: An Emerging Approach to Organic Solar Cells. *Acc. Chem. Res.* **2009**, *42*, 1719–1730.
8. Tamayo, A. B.; Dang, X.-D.; Walker, B.; Seo, J.; Kent, T.; Nguyen, T.-Q. A Low Band Gap, Solution Processable Oligothiophene with a Dialkylated Diketopyrrolopyrrole Chromophore for Use in Bulk Heterojunction Solar Cells. *Appl. Phys. Lett.* **2009**, *94*, 103301–103303.
9. Ma, B. W.; Woo, C. H.; Miyamoto, Y.; Fréchet, J. M. J. Solution Processing of a Small Molecule, Subnaphthalocyanine, for Efficient Organic Photovoltaic Cells. *Chem. Mater.* **2009**, *21*, 1413–1417.
10. Nelson, J. Solar Energy: Solar Cells by Self-Assembly. *Science* **2001**, *293*, 1059–1060.
11. Coakley, K. M.; McGehee, M. D. Conjugated Polymer Photovoltaic Cells. *Chem. Mater.* **2004**, *16*, 4533–4542.
12. Brabec, C. J.; Sariciftci, N. S.; Hummelen, J. C. Plastic Solar Cells. *Adv. Funct. Mater.* **2001**, *11*, 15–26.
13. McCulloch, I.; Heeney, M.; Bailey, C.; Genevicius, K.; Macdonald, I.; Shkunov, M.; Sparrowe, D.; Tierney, S.; Wagner, R.; Zhang, W. M.; *et al.* Liquid-Crystalline Semiconducting Polymers with High Charge-Carrier Mobility. *Nat. Mater.* **2006**, *5*, 328–333.
14. Li, G.; Shrotriya, V.; Huang, J. S.; Yao, Y.; Moriarty, T.; Emery, K.; Yang, Y. High-Efficiency Solution Processable Polymer Photovoltaic Cells by Self-Organization of Polymer Blends. *Nat. Mater.* **2005**, *4*, 864–868.
15. Kim, J. Y.; Lee, K.; Coates, N. E.; Moses, D.; Nguyen, T. Q.; Dante, M.; Heeger, A. J. Efficient Tandem Polymer Solar Cells Fabricated by All-Solution Processing. *Science* **2007**, *317*, 222–225.
16. Sirringhaus, H.; Brown, P. J.; Friend, R. H.; Nielsen, M. M.; Bechgaard, K.; Langeveld-Voss, B. M. W.; Spiering, A. J. H.; Janssen, R. A. J.; Meijer, E. W.; Herwig, P.; *et al.* Two-Dimensional Charge Transport in Self-Organized, High-Mobility Conjugated Polymers. *Nature* **1999**, *401*, 685–688.
17. Ma, W. L.; Yang, C. Y.; Gong, X.; Lee, K.; Heeger, A. J. Thermally Stable, Efficient Polymer Solar Cells with Nanoscale Control of the Interpenetrating Network Morphology. *Adv. Funct. Mater.* **2005**, *15*, 1617–1622.
18. Peet, J.; Heeger, A. J.; Bazan, G. C. "Plastic" Solar Cells: Self-Assembly of Bulk Heterojunction Nanomaterials by Spontaneous Phase Separation. *Acc. Chem. Res.* **2009**, *42*, 1700–1708.
19. Reyes-Reyes, M.; Kim, K.; Carroll, D. L. High-Efficiency Photovoltaic Devices Based on Annealed Poly(3-hexylthiophene) and 1-(3-Methoxycarbonyl)-propyl-1-phenyl-(6,6)C-61 Blends. *Appl. Phys. Lett.* **2005**, *87*, 083506.
20. Huang, E.; Rockford, L.; Russell, T. P.; Hawker, C. J. Nanodomain Control in Copolymer Thin Films. *Nature* **1998**, *395*, 757–758.
21. Kim, S. H.; Misner, M. J.; Xu, T.; Kimura, M.; Russell, T. P. Highly Oriented and Ordered Arrays from Block Copolymers *via* Solvent Evaporation. *Adv. Mater.* **2004**, *16*, 226–231.
22. Thurn-Albrecht, T.; Schotter, J.; Kastle, C. A.; Emley, N.; Shibauchi, T.; Krusin-Elbaum, L.; Guarini, K.; Black, C. T.; Tuominen, M. T.; Russell, T. P. Ultrahigh-Density Nanowire Arrays Grown in Self-Assembled Diblock Copolymer Templates. *Science* **2000**, *290*, 2126–2129.
23. Van Der Veen, M. H.; De Boer, B.; Stalmach, U.; Van De Wetering, K. I.; Hadziioannou, G. Donor−Acceptor Diblock Copolymers Based on PPV and C60: Synthesis, Thermal Properties, and Morphology. *Macromolecules* **2004**, *37*, 3673–3684.
24. Olsen, B. D.; Segalman, R. A. Structure and Thermodynamics of Weakly Segregated Rod−Coil Block Copolymers. *Macromolecules* **2005**, *38*, 10127–10137.
25. Zhu, Z.; Waller, D.; Gaudiana, R.; Morana, M.; Muhlbacher, D.; Scharber, M.; Brabec, C. Panchromatic Conjugated Polymers Containing Alternating Donor/Acceptor Units for Photovoltaic Applications. *Macromolecules* **2007**, *40*, 1981–1986.
26. Sommer, M.; Lang, A. S.; Thelakkat, M. Crystalline−Crystalline Donor−Acceptor Block Copolymers. *Angew. Chem., Int. Ed.* **2008**, *47*, 7901–7904.
27. Sary, N.; Mezzenga, R.; Brochon, C.; Hadziioannou, G.; Ruokolainen, J. Weakly Segregated Smectic C Lamellar Clusters in Blends of Rods and Rod−Coil Block Copolymers. *Macromolecules* **2007**, *40*, 3277–3286.
28. Sary, N.; Rubatat, L.; Brochon, C.; Hadziioannou, G.; Ruokolainen, J.; Mezzenga, R. Self-Assembly of Poly(diethylhexyloxy-*p*-phenylenevinylene)-*b*-Poly(4-vinylpyridine) Rod−Coil Block Copolymer Systems. *Macromolecules* **2007**, *40*, 6990–6997.
29. Sivula, K.; Ball, Z. T.; Watanabe, N.; Fréchet, J. M. J. Amphiphilic Diblock Copolymer Compatibilizers and Their Effect on the Morphology and Performance of Polythiophene:Fullerene Solar Cells. *Adv. Mater.* **2006**, *18*, 206–210.
30. Kato, T.; Fréchet, J. M. J. Stabilization of a Liquid-Crystalline Phase through Noncovalent Interaction with a Polymer Side Chain. *Macromolecules* **1989**, *22*, 3818–3819.
31. Ikkala, O. T.; Laakso, J.; Vakiparta, K.; Virtanen, E.; Ruohonen, H.; Jarvinen, H.; Taka, T.; Passiniemi, P.; Osterholm, J. E.; Cao, Y.; *et al.* Counter-Ion Induced Processibility of Polyaniline: Conducting Melt Processible Polymer Blends. *Synth. Met.* **1995**, *69*, 97–100.
32. Ikkala, O. T.; Pietila, L. O.; Passiniemi, P.; Vikki, T.; Osterholm, H.; Ahjopalo, L.; Osterholm, J. E. Processible Polyaniline Complexes Due to Molecular Recognition: Supramolecular Structures Based on Hydrogen Bonding and Phenyl Stacking. *Synth. Met.* **1997**, *84*, 55–58.
33. Ikkala, O.; Ten Brinke, G. Hierarchical Self-Assembly in Polymeric Complexes: Towards Functional Materials. *Chem. Commun.* **2004**, 2131–2137.

34. Wurthner, F.; Chen, Z. J.; Hoeben, F. J. M.; Osswald, P.; You, C. C.; Jonkheijm, P.; Von Herrikhuyzen, J.; Schenning, A. P. H. J.; Van Der Schoot, P. P. A. M.; Meijer, E. W.; *et al.* Supramolecular p−n-Heterojunctions by Co-Self-Organization of Oligo(*p*-phenylene vinylene) and Perylene Bisimide Dyes. *J. Am. Chem. Soc.* **2004**, *126*, 10611–10618.
35. Tang, C. B.; Lennon, E. M.; Fredrickson, G. H.; Kramer, E. J.; Hawker, C. J. Evolution of Block Copolymer Lithography to Highly Ordered Square Arrays. *Science* **2008**, *322*, 429–432.
36. Antonietti, M.; Conrad, J. Synthesis of Very Highly Ordered Liquid-Crystalline Phases by Complex-Formation of Polyacrylic-Acid with Cationic Surfactants. *Angew. Chem., Int. Ed. Engl.* **1994**, *33*, 1869–1870.
37. Antonietti, M.; Conrad, J.; Thunemann, A. Polyelectrolyte-Surfactant Complexes—A New Type of Solid, Mesomorphous Material. *Macromolecules* **1994**, *27*, 6007–6011.
38. Fyfe, M. C. T.; Stoddart, J. F. Synthetic Supramolecular Chemistry. *Acc. Chem. Res.* **1997**, *30*, 393–401.
39. Van Zoelen, W.; Asumaa, T.; Ruokolainen, J.; Ikkala, O.; Ten Brinke, G. Phase Behavior of Solvent Vapor Annealed Thin Films of PS-*b*-P4VP(PDP) Supramolecules. *Macromolecules* **2008**, *41*, 3199–3208.
40. Van Zoelen, W.; Polushkin, E.; Ten Brinke, G. Hierarchical Terrace Formation in PS-*b*-P4VP(PDP) Supramolecular Thin Films. *Macromolecules* **2008**, *41*, 8807–8814.
41. Tung, S. H.; Kalarickal, N. C.; Mays, J. W.; Xu, T. Hierarchical Assemblies of Block-Copolymer-Based Supramolecules in Thin Films. *Macromolecules* **2008**, *41*, 6453–6462.
42. Tokarev, I.; Krenek, R.; Burkov, Y.; Schmeisser, D.; Sidorenko, A.; Minko, S.; Stamm, M. Microphase Separation in Thin Films of Poly(styrene-*block*-4-vinylpyridine) Copolymer−2-(4′-Hydroxybenzeneazo)benzoic Acid Assembly. *Macromolecules* **2005**, *38*, 507–516.
43. Albrecht, K.; Mourran, A.; Zhu, X. M.; Markkula, T.; Groll, J.; Beginn, U.; De Jeu, W. H.; Moeller, M. Thin Film Morphologies of Block Copolymers Complexed with Wedge-Shaped Liquid Crystalline Amphiphilic Molecules. *Macromolecules* **2008**, *41*, 1728–1738.
44. Kang, J.; Shin, N.; Jang, D. Y.; Prabhu, V. M.; Yoon, D. Y. Structure and Properties of Small Molecule-Polymer Blend Semiconductors for Organic Thin Film Transistors. *J. Am. Chem. Soc.* **2008**, *130*, 12273–12275.
45. Sary, N.; Richard, F.; Brochon, C.; Leclerc, N.; Leveque, P.; Audinot, J. N.; Berson, S.; Heiser, T.; Hadziioannou, C.; Mezzenga, R. A New Supramolecular Route for Using Rod−Coil Block Copolymers in Photovoltaic Applications. *Adv. Mater.* **2010**, *22*, 763–768.
46. Steiner, T. The Hydrogen Bond in the Solid State. *Angew. Chem., Int. Ed.* **2002**, *41*, 48–76.
47. Ruokolainen, J.; Saariaho, M.; Ikkala, O.; Ten Brinke, G.; Thomas, E. L.; Torkkeli, M.; Serimaa, R. Supramolecular Routes to Hierarchical Structures: Comb−Coil Diblock Copolymers Organized with Two Length Scales. *Macromolecules* **1999**, *32*, 1152–1158.
48. Hamadani, B. H.; Richter, C. A.; Gundlach, D. J.; Kline, R. J.; Mcculloch, I.; Heeney, M. Influence of Source−Drain Electric Field on Mobility and Charge Transport in Organic Field-Effect Transistors. *J. Appl. Phys.* **2007**, *102*, 243512.
49. Yu, G.; Gao, J.; Hummelen, J. C.; Wudl, F.; Heeger, A. J. Polymer Photovoltaic Cells: Enhanced Efficiencies *via* a Network of Internal Donor−Acceptor Heterojunctions. *Science* **1995**, *270*, 1789–1791.
50. Blom, P. W. M.; Jong, M. J. M. D.; Vleggaar, J. J. M. Electron and Hole Transport in Poly(*p*-phenylene vinylene) Devices. *Appl. Phys. Lett.* **1996**, *68*, 3308–3310.
51. Geens, W.; Shaheen, S. E.; Wessling, B.; Brabec, C. J.; Poortmans, J.; Serdar Sariciftci, N. Dependence of Field-Effect Hole Mobility of PPV-Based Polymer Films on the Spin-Casting Solvent. *Org. Electron.* **2002**, *3*, 105–110.
52. Dodabalapur, A.; Torsi, L.; Katz, H. E. Organic Transistors: Two-Dimensional Transport and Improved Electrical Characteristics. *Science* **1995**, *268*, 270–271.
53. Dinelli, F.; Murgia, M.; Levy, P.; Cavallini, M.; Biscarini, F.; De Leeuw, D. M. Spatially Correlated Charge Transport in Organic Thin Film Transistors. *Phys. Rev. Lett.* **2004**, *92*, 116802.
54. Mauldin, C. E.; Puntambekar, K.; Murphy, A. R.; Liao, F.; Subramanian, V.; Fréchet, J. M. J.; Delongchamp, D. M.; Fischer, D. A.; Toney, M. F. Solution-Processable α,ω-Distyryl Oligothiophene Semiconductors with Enhanced Environmental Stability. *Chem. Mater.* **2009**, *21*, 1927–1938.
55. Kline, R. J.; McGehee, M. D.; Kadnikova, E. N.; Liu, J.; Fréchet, J. M. J. Controlling the Field-Effect Mobility of Regioregular Polythiophene by Changing the Molecular Weight. *Adv. Mater.* **2003**, *15*, 1519–1522.
56. Friend, R. H.; Gymer, R. W.; Holmes, A. B.; Burroughes, J. H.; Marks, R. N.; Taliani, C.; Bradley, D. D. C.; Santos, D. A. D.; Bredas, J. L.; Logdlund, M.; *et al.* Electroluminescence in Conjugated Polymers. *Nature* **1999**, *397*, 121–128.
57. Zhao, Y.; Thorkelsson, K.; Mastroianni, A. J.; Schilling, T.; Luther, J. M.; Rancatore, B. J.; Matsunaga, K.; Jinnai, H.; Wu, Y.; Poulsen, D.; *et al.* Small-Molecule-Directed Nanoparticle Assembly towards Stimuli-Responsive Nanocomposites. *Nat. Mater.* **2009**, *8*, 979–985.
58. Li, X.; Narayanan, S.; Sprung, M.; Sandy, A.; Lee, D. R.; Wang, J. Developing a Dedicated GISAXS Beamline at the APS. *AIP Conf. Proc.* **2007**, *879*, 1387–1390.